Scanning tunneling microscope light emission: Effect of the strong dc field on junction plasmons

Vijith Kalathingal,[1,*] Paul Dawson,[2] and J. Mitra[1,†]

[1]*School of Physics, Indian Institute of Science Education and Research, Thiruvananthapuram, Kerala 695016, India*
[2]*Centre for Nanostructured Media, Queen's University, Belfast BT7 1NN, United Kingdom*

The observed energies of the localized surface plasmons (LSPs) excited at the tip-sample junction of a scanning tunneling microscope, as identified by spectral peaks in the light output, are very significantly redshifted with respect to calculations that use standard optical data for the tip and sample material, gold in this case. We argue that this anomaly depends on the extreme field in the sub-nm tunneling proximity of the tip and the sample, across which a dc bias (1–2 V) is applied. Finite element modeling analysis is presented of a gold nanosphere-plane (NS-P) combination in tunneling proximity and, crucially, in the presence of a high static electric field ($\sim 10^9$ V/m). It is argued that the strong dc field induces nonlinear corrections to the dielectric function of the gold via the effect of a large background polarizability through the nonlinear, $\chi^{(3)}$ susceptibility contribution. When fed into the model system the modified optical data alters the LSP cavity modes of the NS-P system to indeed reveal a large redshift in energy compared to those of the virgin gold NS-P system. The net outcome may be regarded as equivalent to lowering the bulk plasmon energy, the physical interpretation being that the intense field of the tunneling environment leads to surface charge screening, effectively reducing the density of free electrons available to participate in the plasmon oscillations.

I. INTRODUCTION

It is now 40 years since the first observation of visible light emission due to tunneling electrons—that was in a solid state, metal-oxide-metal device [1]. In this seminal work it was recognized that the emission occurred via the intermediate excitation of plasmon modes in the system, specifically propagating surface plasmon polaritons (SPPs) which were scattered to radiation via surface roughness features. With random roughness the emission is broadband in nature, the output bearing the spectral imprint of the optical properties of the top electrode (emission-side) metal [2]; alternatively, the output color could be made angle-tunable by the impressing of a periodic grating profile on the tunnel junctions [3,4]. A further interesting development of this physical mechanism of light generation was the harnessing of emission from localized surface plasmons (LSPs) supported on nanoscale Ag particles separated by a thin dielectric spacer layer from an underlying metal-oxide-metal tunnel junction [5].

In 1988 Gimzewski *et al.* [6] reported the LSP-mediated emission of light from a scanning tunneling microscope (STM) where, in contrast to the LSPs of stand alone metal particles reported in Ref. [5], the LSPs were those associated with a coupled metal-tip/metal-sample tunnel gap. Since then there have a been a number of experimental and theoretical investigations of this phenomenon [7–14]. For a Au/Ag STM junction the emission is known to span the spectral range from visible to near infrared, with the lower wavelength (maximum energy) cutoff decided by the applied dc bias. The importance of STM light emission (STMLE) stems not only from the fact that it is one of the few techniques that affords study of electron excited plasmons, but one that provides a highly flexible platform in which the energy and intensity of the junction plasmons may

be tuned continuously [15–18]. Notably, excitation of SPPs [19,20] has also been demonstrated with the STM in addition to that of LSPs, confined at the tip-sample junction (TSJ) [9,13,21]. Molecular tunnel junctions which act as electrically controlled plasmon sources offer future directions to electronic circuits in the nanoscale combined with plasmonics [22]. Le Moal *et al.* have shown that low-energy electrons tunneling from a sharp tungsten tip to a single gold nanoparticle (NP) realize a nanoscale light source with a controllable emission pattern, devoid of background radiation excitation [23]. It is the lure of this literal "dark field"imaging and spectroscopy that makes STMLE so attractive a phenomenon to study.

The optoelectronic properties of a STM-TSJ is closely mimicked by the nanosphere-plane (NS-P) system (Fig. 1), which has been extensively exploited to model and investigate the physics of coupled or junction plasmons [24–32]. For metal-metal STM-TSJs, the junction LSPs are understood to be excited by tunnel current fluctuations, a fraction of which then decay emitting light [8]. Invoking optical reciprocity, information about the same LSP modes may be obtained from the NS-P system using incident electromagnetic excitation, where peaks in the electric field enhancement factor E_f versus frequency (wavelength) indicates the LSP modal energies [33]. However, all previous investigations into modeling the STMLE have ignored a crucial aspect of STM experimentation, the strong dc electric field ($\sim 10^9$ V/m) that permeates the STM junction. Not only is the surrounding dielectric medium (vacuum or otherwise) subject to this robust dc field but the tip end and the sample below are also subject to the same. Our present study focuses on the NS-P modeling of plasmon mediated STMLE spectra with relevance to related applications ranging from single molecule detection [17,18] to lithography [34]. Allied spectroscopic techniques like tip-enhanced Raman scattering (TERS) that provides chemical fingerprint of molecules require a complete understanding of the cavity LSP modal energies [18], especially in the presence of the dc field.

*vijith@iisertvm.ac.in
†j.mitra@iisertvm.ac.in
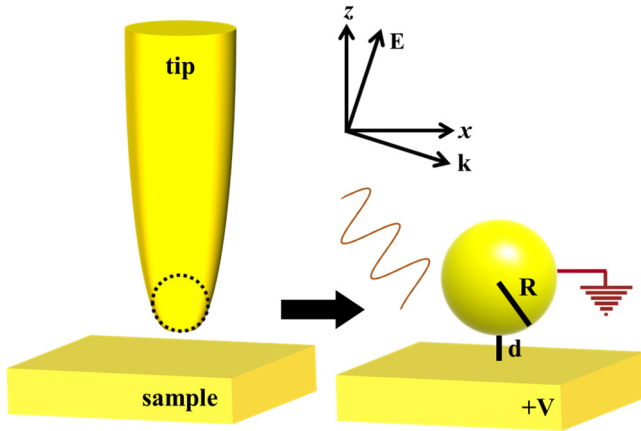
FIG. 1. The STM tip-sample junction (left) and the equivalent nanosphere-plane system (right). Incident electric field (**E**) polarized at 20° with normal ($\hat{z}$).

It has been known that the energies of the junction plasmon modes may be systematically controlled by tuning either the geometric properties (e.g., tip end or NS radius and tip-sample separation) or the dielectric properties of the TSJ environment [24–26,30]. Specifically, previous attempts at modeling STMLE spectra necessitated an overall redshift of the calculated spectra, to obtain a match between theoretical and experimental data. The redshift has been variously effected by an anomalous lowering of the bulk plasmon energy ($\hbar\omega_p$) to $\sim$3.6 eV [35], much lower than the bulk value of $\sim$8 eV [36] or including contributions from polarizable core electrons [37]. Here, we probe the effect of the dc bias on the junction of a Au-Au NS-P system by incorporating nonlinear corrections to the local dielectric function of the metal due to the intense dc field ($\sim10^9$ V/m) at the junction. Finite element method modeling has been used to simulate the NS-P system and calculate its effective plasmonic response with a plane polarized electromagnetic wave incident at 20° to the vertical (Fig. 1). Additionally, if a strong dc electric field is superimposed onto the junction, strongly polarized matter around the junction (i.e., the tip and sample) will affect the coherent oscillations of the *free* electrons between the tip and sample, that sustain the LSPs. Section II below elucidates the theoretical analysis based on third-order optical nonlinearity followed by the relevant results and discussion in Sec. III. The STMLE spectra presented here have been acquired with chemically etched Au tips [38] on single crystalline Au(111) surfaces with a bias of +1.8 V applied to the sample. Further details about the experimental setup are available in Refs. [14,35].

II. METHODS AND THEORETICAL BACKGROUND

Within our energy range of interest typically 0.7–2.0 eV (corresponding to STMLE in the visible and near IR, 600–1600 nm) the dielectric properties of Au are rather well described by the Drude free-electron theory with the dielectric function given by

$$\varepsilon(\omega) = \left\{ \epsilon^0 - \frac{\omega_p^2}{(\omega^2 + \gamma_D^2)} \right\} + i \left\{ \frac{\omega_p^2 \gamma_D}{\omega(\omega^2 + \gamma_D^2)} \right\}, \quad (1)$$

where ω_p is the bulk plasma frequency, γ_D is the damping constant, and $\epsilon^0 = 1$ [39], within the free-electron model. The plasmonic response of isolated nanoparticles or stand alone thin films of Au or Ag are well modelled [40–42] using either the standard experimental dielectric data or their equivalent fit with the Drude dielectric function [Eq. (1)]. For Au, the the Drude model with $\omega_p \sim 8$ eV and $\gamma_D \sim 0.1$ eV [43] provides an excellent match to the experimental data [44] for energies up to $\sim$2 eV, beyond which significant deviations are observed, especially in the imaginary component. However, the same dielectric data, either experimentally obtained or its theoretical fit, do not accurately reproduce the experimental observations in the context of localized gap plasmons, in the energy range 0.5–2 eV for Au. This mismatch has been mainly ascribed to the presence of the polarizable core electrons, i.e., the completely filled d band [25,28,37], where contribution to the dielectric function has been incorporated by including a large positive value for ϵ^0, resulting in an agreement between theoretical calculations and experimentally obtained optical absorption or extinction spectra [25,28]. Incorporating a large positive value for $\epsilon^0 (>1)$ in Eq. (1) also results in an apparent decrease in the observed plasma frequency [25]. For Ag, the corrected plasma frequency is reduced to 3.9 eV from 9.2 eV, inducing transparency at much longer wavelengths than theoretically predicted [45]. The discrepancy is accentuated while modeling the STMLE spectra, where calculating the LSP modal energies of the TSJ is central to the investigation. Most attempts at modeling the experimentally detected emission spectra have resulted in only a qualitative match, with reasonable predictability of spectral dependence on the associated parameters, e.g., geometrical properties of the TSJ, dielectric function of the environment, etc. Our previous attempts at modeling STMLE spectra with a phenomenological model [14] based on the LSP modal energy calculation of Rendell and Scalapino [33] and also a more direct finite element modeling study [35], using the Drude dielectric function, have indicated that the experimentally observed spectra are grossly redshifted compared to their theoretical counterpart. Interestingly though, an excellent match is obtained between theory and experiment in either of the above methods, if an effectively lowered $\hbar\omega_p \sim$ 3.5–4.0 eV is used in Eq. (1) with $\epsilon^0 = 1$. The reduction in $\hbar\omega_p$ effectively rescales the calculated plasmon modes resulting in an overall redshift of the calculated spectra, more quantitatively matching experimental data than afforded before. The reduced $\hbar\omega_p$ has been variously justified as originating from quantum size effects, core electron contribution, and reduced number density of free electrons in nanoparticles.

Recently, there have been a number of theoretical studies on calculating the plasmonic modes of metal nanostructures in tunneling proximity, typically with separations of 0.3 nm, or smaller [46]. The studies have mainly focused on two aspects, first incorporating quantum corrections [47,48] within the classical calculation of the electromagnetic response and, second, incorporating nonlocal corrections [29] in defining the dielectric properties of the constituent nanostructures. It is well known that for NS-P or NS-NS systems the LSP modes redshift with decreasing separation, however as the system enters the quantum regime the modes have been shown to blueshift with further decrease in separation. Theoretical calculation of the emission spectra from the STM-TSJ is further complicated

by two factors: first the tunneling proximity, along with substantial charge transfer between the tip and sample and the large dc bias permeating the junction.

In general, the response of conduction or *free* electrons in metals, to an external electric field (**E**), is not linear, though the nonlinear effects are only manifest in the high-field regime [49,50]. In the low field, linear regime the polarization (**P**) of a media may be written as $\mathbf{P} = \varepsilon_0 \chi \mathbf{E}$, where ε_0 is the permittivity of free space and χ is the material susceptibility. For a majority of nonlinear systems **P** may be expressed as a power series of the form

$$\mathbf{P} = \varepsilon_0[\chi^{(1)}\mathbf{E} + \chi^{(2)}\mathbf{E}^2 + \chi^{(3)}\mathbf{E}^3 + \cdots] \qquad (2)$$

$\chi^{(\iota)}$ being the ιth-order material susceptibility. For centrosymmetric systems a Kerr type nonlinearity leads to the modified dielectric function for the material given as [51]

$$\varepsilon = 1 + \chi^{(1)} + 3\chi^{(3)}|\mathbf{E}|^2. \qquad (3)$$

The above, though more commonly evidenced in the context of ac electric fields, has also been observed for strong dc electric fields [49]. The TSJ in the STM is permeated by such a strong dc electric field, originating from the applied dc bias across the sub-nm tunnel gap. In spite of the applied dc bias the resulting tunnel current is not purely dc but incorporates a fluctuating component [52]. This fluctuating component may be seen as corresponding to a fluctuating electric field and an oscillating charge density between the tip and sample, evidenced as LSPs within the tunnel junction. This intense dc field, localized within the TSJ, affects only the tip endpoint and the sample directly below and may significantly alter the local electron distribution and its dynamics, departing from the typical *free*-electron response that is reflected in the local dielectric function. Any such modification will be confined only to the extreme vicinity of the junction and not extend beyond a relevant length scale. In bulk metals, external dc electric fields typically penetrate up to the Thomas-Fermi screening length (λ_{TF}) [39]. The electron screening effects in nanoparticles, of a few nanometers in dimension, are markedly different from their bulk counterpart due to their restricted number density and damping [53]. It is the latter which is more applicable in the context of the STM-TSJ, where the screening effects of the small volume around the TSJ crucially decides the physics of the junction LSPs.

Detailed analysis based on the classical model of optical nonlinearities of an anharmonic oscillator [49] in the presence of an ac field superimposed with a dc field gives the frequency dependent real and imaginary parts of the third-order susceptibility in terms of the first-order term. The linear susceptibility is analytically found to be

$$\chi^{(1)}(\omega) = \frac{n_e e^2/\varepsilon_0 m}{\omega_0^2 - \omega^2 - 2i\gamma\omega}, \qquad (4)$$

where ω_0 is the natural frequency of oscillation, n_e is the electron number density, and γ is the damping coefficient. For a combined dc($\omega = 0$) and ac field, $\chi^{(3)}$ may be written as

$$\chi^{(3)}(\omega) = b[\chi^{(1)}(0)]^2[\chi^{(1)}(\omega)]^2, \qquad (5)$$

where the parameter b quantifies the strength of the nonlinearity. To a first-order approximation assuming $\chi^{(1)}(\omega) = \varepsilon - 1$,

with ε given by the Drude result,

$$\chi^{(3)}(\omega) = \chi^{(3)}_{\text{real}}\omega_p^4\left(\frac{1}{(\omega^2 + \gamma^2)^2} - \frac{\gamma^2}{\omega^2(\omega^2 + \gamma^2)^2}\right)$$
$$- i\left(\frac{\chi^{(3)}_{\text{imag}}\omega_p^4\gamma}{\omega(\omega^2 + \gamma^2)^2}\right), \qquad (6)$$

where $\chi^{(3)}_{\text{real}}$ and $\chi^{(3)}_{\text{imag}}$ are constants depicting the strength of nonlinearity which takes account of the factor b. Evidently, the damping coefficient γ plays a critical role in determining the behavior of $\chi^{(3)}(\omega)$ and its frequency dependence. The above expression may be used in conjunction with Eq. (3) to obtain a modified dielectric function [54],

$$\Sigma(\omega) = 1 - \frac{\omega_p^2}{(\omega^2 + \gamma^2)} + 3\chi^{(3)}_{\text{real}}\omega_p^4\mathbf{E}^2$$
$$\times \left(\frac{1}{(\omega^2 + \gamma^2)^2} - \frac{\gamma^2}{\omega^2(\omega^2 + \gamma^2)^2}\right)$$
$$+ i\left(\frac{\omega_p^2\gamma}{\omega(\omega^2 + \gamma^2)} - \frac{3\chi^{(3)}_{\text{imag}}\omega_p^4\gamma\mathbf{E}^2}{\omega(\omega^2 + \gamma^2)^2}\right). \qquad (7)$$

The commercial software package COMSOL Multiphysics 5® intended for 3D finite element modeling was employed to simulate the electromagnetic response of NS-P system in the classical domain. The simulation geometry, shown in Fig. 1, consists of a spherical particle of radius R separated by a distance d from a semi-infinite substrate of lateral dimension $10R$ and thickness t. For a typical STM tip-sample geometry the spacing d was chosen to be 1 nm with a substrate thickness of $t = 25$ nm, which is larger than the optical skin depth of Au to eliminate any thickness dependent effects on LSP modal energies [25]. The built-in electrostatic and electromagnetic module of the simulation package was adopted for the present study coupled with each other. The spatial variation of the dc field is calculated for a 1.8-V bias applied to Au substrate with the Au NS surface held at zero potential. The LSP modes of the nanocavity are then evidenced as the local-field enhancement in ac electromagnetic response at the junction [35]. The simulation domain is considered to be free space ($\epsilon = 1.0$). Spatially graded meshing is applied to maximize the mesh density at the junction while keeping the total number of nodes low. Analytically obtained dielectric function [Eq. (7)] with $\omega_p = 8$ eV is used (other parameters are given in the discussion) to represent the optical properties of Au tip and substrate.

III. RESULTS AND DISCUSSION

Figure 2(a) (dash-dot line) plots the variation of the calculated dc electric field along NS surface, for a 25-nm tip, with the substrate held at 1.8-V bias. Zero of the x axis is taken as the point of closest approach of the NS-P system. The inset shows the NS-P system in yellow along with the spatial variation of the dc field around the junction. While the maximum field value is primarily decided by the junction separation (d), the lateral spread is a function of the tip-end curvature. Having calculated the dc field at all points on the surface of the NS-P system we assume that the screened field at a point in the interior is given by the expression [55]

$$E(r,\theta) = E_S(0,\theta)e^{-r/\eta}, \qquad (8)$$

(a)

(b)

(c)
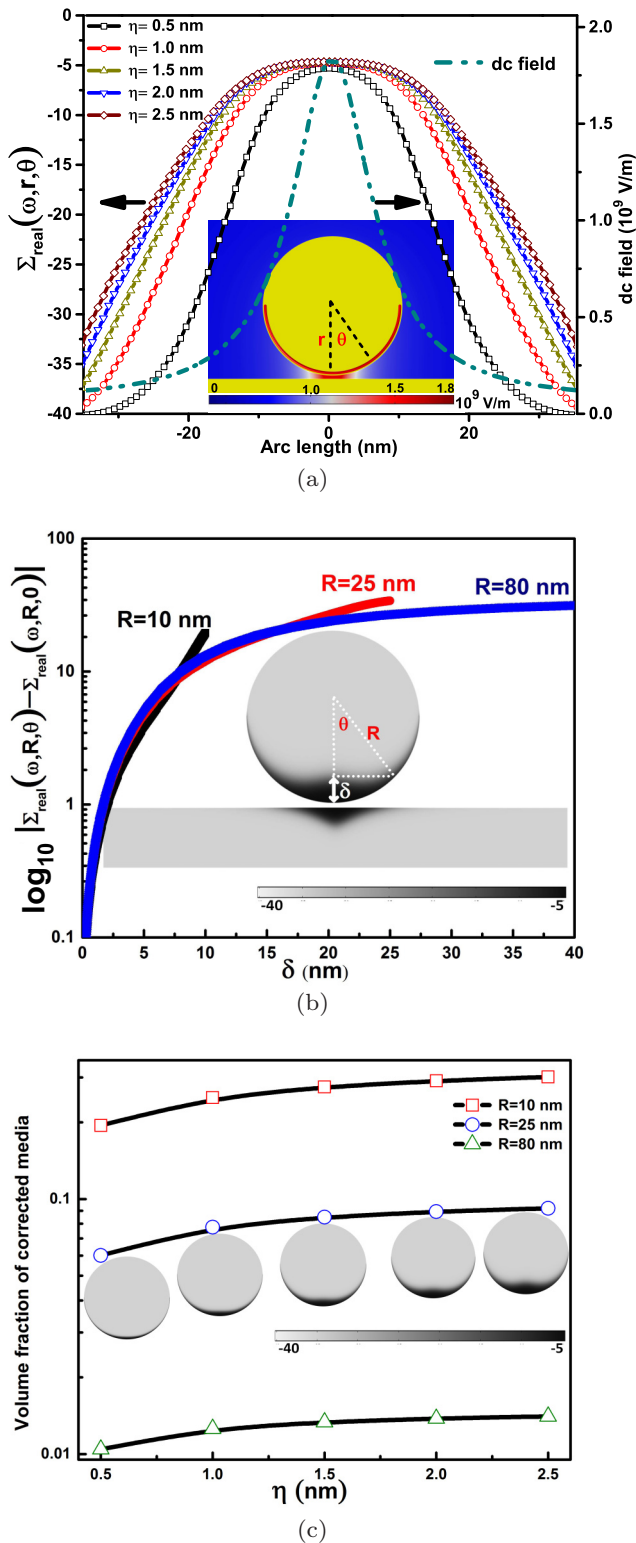
FIG. 2. (a) $\Sigma_{\mathrm{real}}(\omega,r,\theta)$ (left) and dc field variation (right) plotted as a function of arc length (red arc in the inset) for different η (inset: spatial variation of dc field for NS-P system). (b) $\Sigma_{\mathrm{real}}(\omega,R,\theta)$ plotted as a function of δ (see text) for three tip radii for $\eta = 2.5$ nm and $\lambda = 1000$ nm (inset: cross-sectional plots $\Sigma_{\mathrm{real}}(\omega,r,\theta)$ for 25 nm NS-P system). (c) Variation of the volume fraction of the corrected media (see text) for tip radii 10, 25, and 80 nm as a function of η (inset: cross-sectional plots of Σ_{real} within the 25-nm tip for $\lambda = 1000$ nm, showing variation of the corrected volume).

where $E_S(0,\theta)$ is the dc field at the metal surface, η is an adjustable parameter, r is the distance to an interior point from surface. For the NS $r = 0$ denotes a point on the surface and $\theta = 0$ at the point of closest approach, i.e., the TSJ [Fig. 2(a)]. The field penetration into the sample is modelled identically. The parameter η is finally adjusted such that the resulting electric field inside the material, used to calculate the local dielectric function $\Sigma(\omega)$ [Eq. (7)], reproduces the necessary plasmonic response observed experimentally. In a bulk system, η would be close to the λ_{TF}. Since $\Sigma(\omega)$ is a function of r and θ, the strongest nonlinear correction to $\Sigma(\omega,r,\theta)$ occurs on the NS-P surface at their point of closest approach, i.e., at the junction, and decays symmetrically to the standard Drude value [Eq. (1)] deeper into the metal. This spatially varying $\Sigma(\omega,r,\theta)$ demarcates a small *active* volume within the metals, closest to the junction, within which the dielectric function is substantially corrected. It is the geometry and physics of this active volume that decides the energetics of the junction LSP modes. Figure 2(a) also shows the variation of $\Sigma_{\mathrm{real}}(\omega,r,\theta)$ along the lower surface of a 25-nm NS [along the red arc in the inset of Fig. 2(a)], with η as a parameter. The plots demonstrate that the spatial variation of the dc field, along with η and R, defines an "opening angle" of that active volume, with the physical tip end curvature given by R. This is analogous to the findings of Aizpurua *et al.* [56] where the spectral shape of the STMLE emission spectra was found to be strongly dependent on similar parameters, via an opening angle that was defined purely in geometrical terms. The radius of the NS primarily decides the lateral extent of interaction between the NS and the plane. Thus with increasing R the lateral extent of the active volume increases proportionally, however our calculations show that the thickness or depth of this active volume is rather weakly dependent on the radius. Figure 2(b) plots the variation of $\Sigma_{\mathrm{real}}(\omega,R,\theta)$, the real component of the corrected dielectric function at the surface of the tip, with a parameter $\delta\{= R[1 - \cos(\theta)]\}$, for all three NSs of R (=10, 25, and 80 nm). Note that $\delta = 0$ corresponds to $\theta = 0$, i.e., the TSJ. Each curve has been offset by its value at $\theta = 0$ for comparison. The physical relevance of δ is understood from the inset of Fig. 2(b) that shows the variation of the corrected $\Sigma_{\mathrm{real}}(\omega,r,\theta)$ in the NS-P system, around the junction for a 25-nm NS. Calculated for $\eta = 2.5$ nm and $\hbar\omega \equiv 1000$ nm, the darker shades denote stronger corrections with lighter shades denoting values closer to those given by the uncorrected Drude model. The plots demonstrate the weak dependence of the depth of the active volume on R and that the strongest correction occurs for δ varying between 0 and 5 nm, irrespective of the NS radius. Figure 2(c) plots the variation of the active volume fraction for the three NSs with the parameter η. Since the maximum correction occurs at the TSJ ($r = 0$, $\theta = 0$), the relevant volume fraction is evaluated as the volume within which $\Sigma_{\mathrm{real}}(\omega,r,\theta)$ decays to $1/e$ fraction of its magnitude at the TSJ. Figure 2(c) inset shows the variation of the active volume (black shaded region) with η for the 25-nm NS. The active volume fraction increases with η, directly affecting the energetics of the LSP modes, before saturating for $\eta \gtrsim 2$ nm. In the simulations for the three spheres of radii 10, 25, and 80 nm, η is varied from 0.5 to 2.5 nm to match the cavity modes with experimentally observed peak positions (see below). The above analysis shows that it is the shape, size, and dielectric

properties of this corrected effective volume that participates in LSP excitation and controls its energetics, making the physical geometry of the TSJ secondary. The calculated real and imaginary values of the modified $\Sigma(\omega, r, \theta)$ indicates that incorporating the nonlinear correction, promotes ac field (electromagnetic) penetration into the metals, at least over the energy range investigated.

Accommodating nonlinear effects to modify local dielectric properties to model the TSJ LSP modes is a significant departure from the existing models. It is with this scheme that we calculate the dielectric properties of the corrected media in our model for all three cases of tip radii studied. Physically the high dc field strongly polarizes the TSJ thereby reducing the local free-electron density (n) from its bulk value and also adversely affecting the local damping coefficient (γ_D), in the vicinity of the TSJ. Both effects manifest as an increase in the effective inertia of the electrons closest to the TSJ, deviating from their free-electron nature. Equivalently, either of the above changes is analogous to reducing the plasma frequency (ω_p), locally. It is also worth noting that in STMLE the applied bias polarity has no effect on the experimentally detected emission spectrum, i.e., the spectrum is not dependent on the direction of the dc field at the junction. In spite of the asymmetric static charge distribution created at the TSJ, it is the effective *free*-electron density and its properties in material at the TSJ that decides its plasmonic response. This experimentally observed independence of the emission spectrum with respect to bias polarity underlies the justification of applying a Kerr type nonlinearity [Eq. (3)] that is applicable to a centrosymmetric system in the present context.

Finite element modeling of LSP modes of the Au NS-P system, either using the uncorrected Drude model [$\omega_p \sim 8.0$ eV, Eq. (1)] or with the experimental dielectric data [44], results in plasmon modes near 400 nm but none between 600 and 1600 nm (2.06–0.77 eV), as shown in Fig. 3(a) (square dotted line). Experimentally though several LSP modes (peaks) and STMLE may be observed in the above range, dependent on the tip geometry [13,16,35,57]. As mentioned before, an excellent match between theory and experiment may be obtained assuming an anomalous lowering of the $\omega_p \sim 3.6$ eV [35], in the theoretical calculations, which results in an effective redshifting of the plasmon modes into our energy range of interest. Such a redshift of the plasmon modes may also be effected theoretically by incorporating a polarizable electron core in the calculations [37]. Either way it provides credibility to the concept that local changes to the dielectric properties of the TSJ may induce the necessary shift in the theoretically calculated spectra to match experimental results. For an ideal conducting sphere in an external electrostatic field, the induced charges reside over a surface of zero thickness, resulting in zero-field penetration. In real metals the extent of penetration is decided primarily by the carrier density [58], which may be calculated semiclassically for a free-electron gas, as the λ_{TF} [39,59]. It provides the typical length scale over which induced volume charge density is distributed, in the bulk of the material. However, in the context of a TSJ characterized typically by nanometric length scales along with a large permeating dc electric field, the fundamental assumptions of dielectric linearity and slow spatial variation of the external potential becomes rather ill-founded. Consequently, the induced charge

density may not be restricted to a volume dictated by λ_{TF}, but be more delocalized. This active volume around the TSJ is the region over which we assume the external dc field to substantially modify the dielectric properties such that it departs significantly from the bulk values.

The STM-TSJ is further complicated due to quantum tunneling, where explicit charge transfer takes place between the tip and sample, which are neglected here and we restrict ourselves to purely classical calculations. A legacy of the strong polarization of the TSJ is also evidenced through a correction to the damping coefficient, as discussed earlier. We have assumed that the damping constant is locally modified as $\gamma = \gamma_D + KE(r, \theta)$, where K is an adjustable positive parameter, making γ larger than γ_D, within the active volume. Such an increase of γ has been exploited previously in the context of calculating the plasmonic response of two nanoparticles in tunneling proximity [47], where a fictitious media with a high γ was assumed to characterize the tunnel gap.

In simulating the plasmonic response of the NS-P system the decaying dc field [Eq. (8)] inside the NS is used in calculating the corrected dielectric constant $\Sigma(\omega, r, \theta)$ [Eq. (7)], where $\chi^{(3)}$, η, and K appear as parameters. For the real and imaginary values of $\chi^{(3)}$, it is worth referring to a recent report by Boyd *et al.* on the nonlinear susceptibility $\chi^{(3)}$ of gold [50]. The presence of the third-order nonlinear susceptibility of gold cannot emerge from a linear theory like the Drude model, applicable only for an ideal free-electron gas. But if the electrons are confined to a restricted region, either physically within a nanoparticle or around the TSJ by a strong electric field, the same *free electrons* may display nonlinear effects [60]. Further contributions to the nonlinearity may also arise from excitations of $5d$ electrons to the $6sp$ levels, which are not expected to be significant compared to the confinement effect in the present case. Experimental results show that the observed values of $\chi^{(3)}$ span more than three orders in magnitude, typically between 10^{-17} and 10^{-20} m^2/V^2 [50]. The values chosen for our model fit into this numerical regime and are given as follows: $\chi^{(3)}_{\text{real}} \sim 6 \times 10^{-20}$ m^2/V^2; $\chi^{(3)}_{\text{imag}} \sim 2.3 \times 10^{-19}$ m^2/V^2. Similarly, we have used $K = 9.2 \times 10^{-9}$ commensurate with a damping coefficient of a highly resistive tunnel junction. Finally, η was varied until the calculated spectra matched the experimentally obtained emission. The STM-TSJ LSP modes are calculated based on the reciprocity relation that the electromagnetic field at infinity produced by the tunnel current fluctuations is equivalent to the local-field enhancement at the TSJ produced by an external source at infinity [33]. The LSP modes are identified as the peaks in the normalized junction electric field vs wavelength (or energy) plot. Evolution of the calculated spectra with η for the 10-nm NS is shown in Fig. 3(a) with the inset depicting the evolution of the peak positions for each LSP mode number (designated on the basis of increasing energy) as a function of η. The lowest energy (0th) mode moves from 620 to 849 nm as η is varied from 0.5 to 2.5 nm. Similarly the first-order mode evolves from 638 to 674 nm. For comparison, the same spectrum calculated for the uncorrected dielectric function (Drude model with bulk plasmon energy of $\hbar\omega_p = 8$ eV) is also shown in the plot (green line with square dots). The spectrum is conspicuous by the absence of any LSP modes

(a)

(b)

(c)

(d)
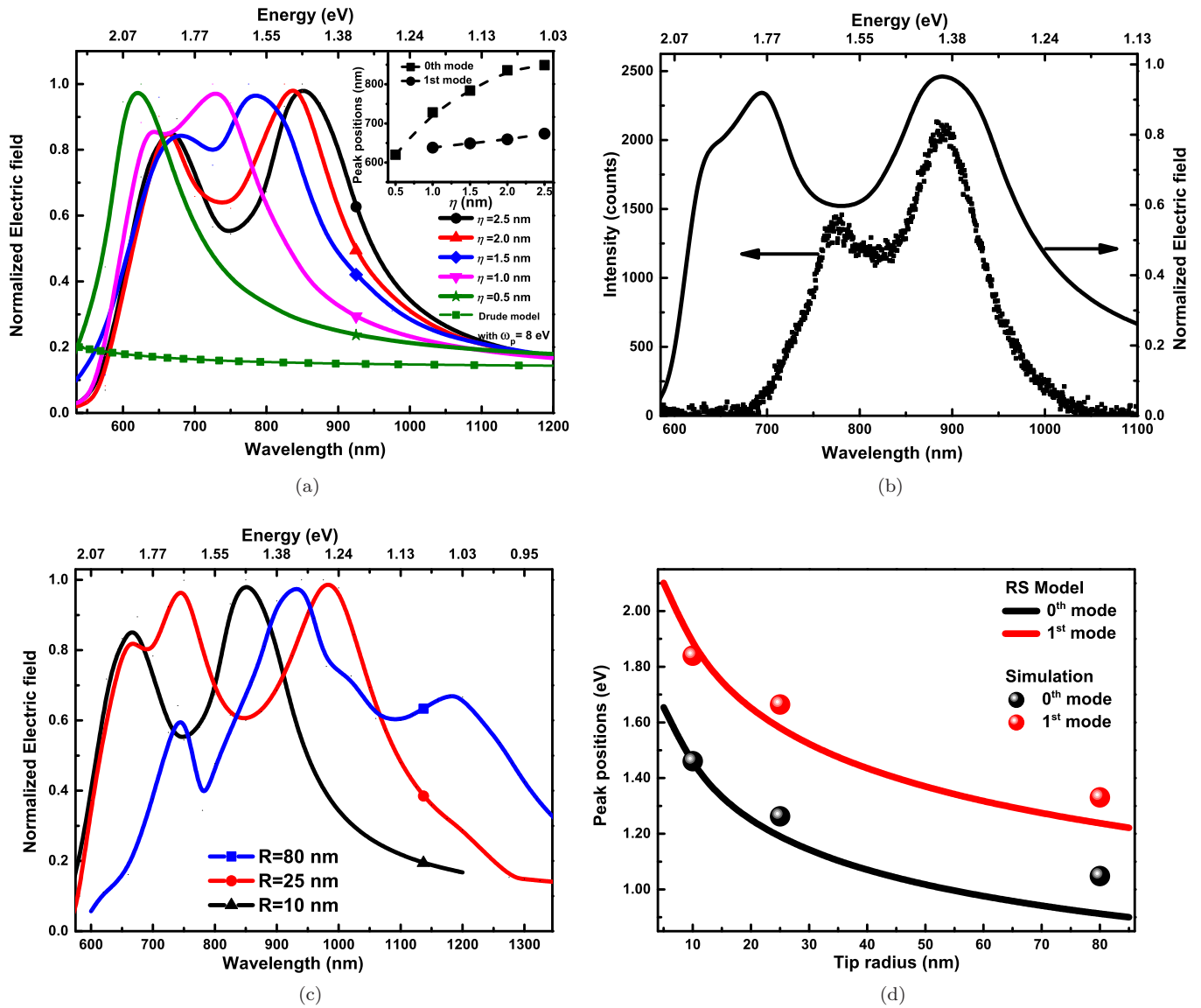
FIG. 3. (a) Normalized electric field calculated 0.1 nm below the tip ($R = 10$ nm) (Inset: evolution of LSP mode positions as a function of η. The dashed lines are a guide to the eye.) (b) Calculated spectra (black solid line) and emission spectra from STMLE experiment (black dots) for 10-nm tip. (c) Calculated spectra for $R = 10$, 25, and 80 nm tip for $\eta = 2.5$ nm. (d) Shift in peak positions with radius of the tip ($\eta = 2.5$ nm). Solid lines shows calculated mode evolution from RS model (see text).

between 2.0 and 0.5 eV, as discussed earlier [14,21]. In the present model an increasing η also increases the active volume of the corrected media around the TSJ, resulting in a redshift of the LSP spectra. Figure 3(b) plots the calculated spectrum ($\eta = 2.5$ nm and $\chi_{\text{real}}^{(3)} = 5.5 \times 10^{-20}$ m^2/V^2) along with that obtained experimentally for a Au-Au junction, biased at 1.8 V with a tunnel current $=10$ nA for a tip end radius ~ 10 nm. The calculated spectrum shows two distinct peaks at $\lambda \sim 680$ nm and at $\lambda \sim 900$ nm, which we refer to as the first- ($\hbar\omega_1 = 1.82$ eV) and zero-order ($\hbar\omega_0 = 1.37$ eV) LSP resonances, respectively. The zero-order peak is evidenced by the peak at $\lambda \sim 900$ nm in the experimental spectrum. Since the emission spectrum was recorded with a tip-sample bias of 1.8 V, it is weighted by the quantum cutoff, theoretically given by the expression $(1 - \hbar\omega/eV_{\text{bias}})$ [33] for $\hbar\omega \leqslant eV$, quenching all emission below 680 nm. Consequently, the

STMLE first-order peak is never fully evidenced in the emission spectrum. The smaller "false" peak at 780 nm is an artefact of the quantum cutoff interfering with the rising edge of the emission towards the lower wavelengths. Though the strength of $\eta = 2.5$ nm is physically motivated, i.e., to effect a match between the experimental and theoretical results, it is worth noting that the variation of the peak positions with η becomes negligible around the same value [Fig. 3(a) inset]. It denotes a self-consistency of the calculations yielding a resultant η, with further changes producing negligible redshifts to the calculated spectra. Importantly, the saturation of the redshift of the modes with η occurs around 2.5 nm for all cases. Figure 3(c) shows the calculated spectra for all three NS-P systems for $\eta = 2.5$ nm. The plots show a redshift of the calculated spectrum with increasing NS size, which is characteristic of junction LSPs [24]. Compared to the

10- and 25-nm cases, the calculated modes for the 80-nm NS are relatively more redshifted with several closely spaced modes at higher energies indicating that the evolution of modes are not uniform over the energy range investigated. Specifically lower energy modes are much more sensitive to η compared with higher energy modes. Overall the general properties of STMLE spectra, viz., peaks in the visible range and redshift and increase in number of LSP modes with increasing R, are preserved in our model [13,14,56,61]. Changes in the shape of the spectra in terms of relative peak positions [Fig. 3(a) inset], confirms the role of η as a curvature parameter. An earlier phenomenological model by Rendell and Scalapino (RS) [33] used to calculate the LSP modes of noble metal TSJ have shown excellent agreement with experimental results in the past [14,21,35]. In the RS model the LSP modes (ω_m) for $d/R \ll 1$ are given by the equation

$$\omega_m = \omega_p \left[\frac{\tanh\left(m + \frac{1}{2}\right)\beta_0}{\epsilon + \tanh\left(m + \frac{1}{2}\right)\beta_0} \right]^{1/2}, \quad m = 0,1,2\ldots, \quad (9)$$

where $\beta_0 = \cosh^{-1}(1 + d/R)$, ϵ is the dielectric function of the medium around TSJ, and m denotes the mode number. Figure 3(d) plots the variation in the calculated mode position, for the 0th and 1st modes, as a function of tip radius for the RS model with $\omega_p = 3.6$ eV along with those from the present simulation, for $\eta = 2.5$ nm. Evidently, the modal positions from simulations follow the same trend with R as given by the RS model.

Figure 4(a) shows the experimentally obtained STMLE emission spectra for various tunnel currents (I_T) at a fixed bias voltage of 1.8 V, for a tip of end point radius $\sim$10 nm. Decreasing the tunnel current at a fixed bias effectively increases the tip-sample distance d. Experimentally a reduction in the tip-sample separation results in (i) a blueshift of the emission spectra and (ii) a decrease in the emission intensity. To calculate the effect of d in the present model the junction electric-field enhancement was calculated as a function of d as shown in Fig. 4(b). Assuming that $d \sim 1$ nm separation correspond to the case of highest tunnel current (40 nA) in Fig. 4(a), the higher values of d corresponding to lower currents were obtained from a one-dimensional (1D) calculation of the STM tunnel current. The correspondence in evolution of the spectra obtained experimentally [Fig. 4(a)] and theoretically [Fig. 4(b)] is more than a mere qualitative match. Figure 4(c) shows the evolution of the peak position of the lowest energy peak with d from the theoretical calculation along with that obtained experimentally, plotted as a function of $\ln(I_T)$ since I_T is exponentially dependent on d. The spatial variation of the LSP modes around the TSJ is of relevance for various practical applications of STMLE and TERS. The scatter plots in Fig. 5 show the lateral variation of the normalized field at the junction for the three NSs, for all LSP modes in the energy range 1.77–1.00 eV (wavelength range 700–1240 nm). The field intensity decays exponentially away from the junction, as evidenced by the exponential fits (solid lines) shown in Fig. 5. The localization length (λ_l) of the LSPs, below the STM tip, may be then calculated as the lateral distance from the center at which $|\mathbf{E}_f|^2$ falls to 50% of its maximum value. Variation of λ_l with R is plotted in the inset of Fig. 5. The RS model predicts λ_l to vary as $\sqrt{2Rd}$ [33]

(a)

(b)

(c)
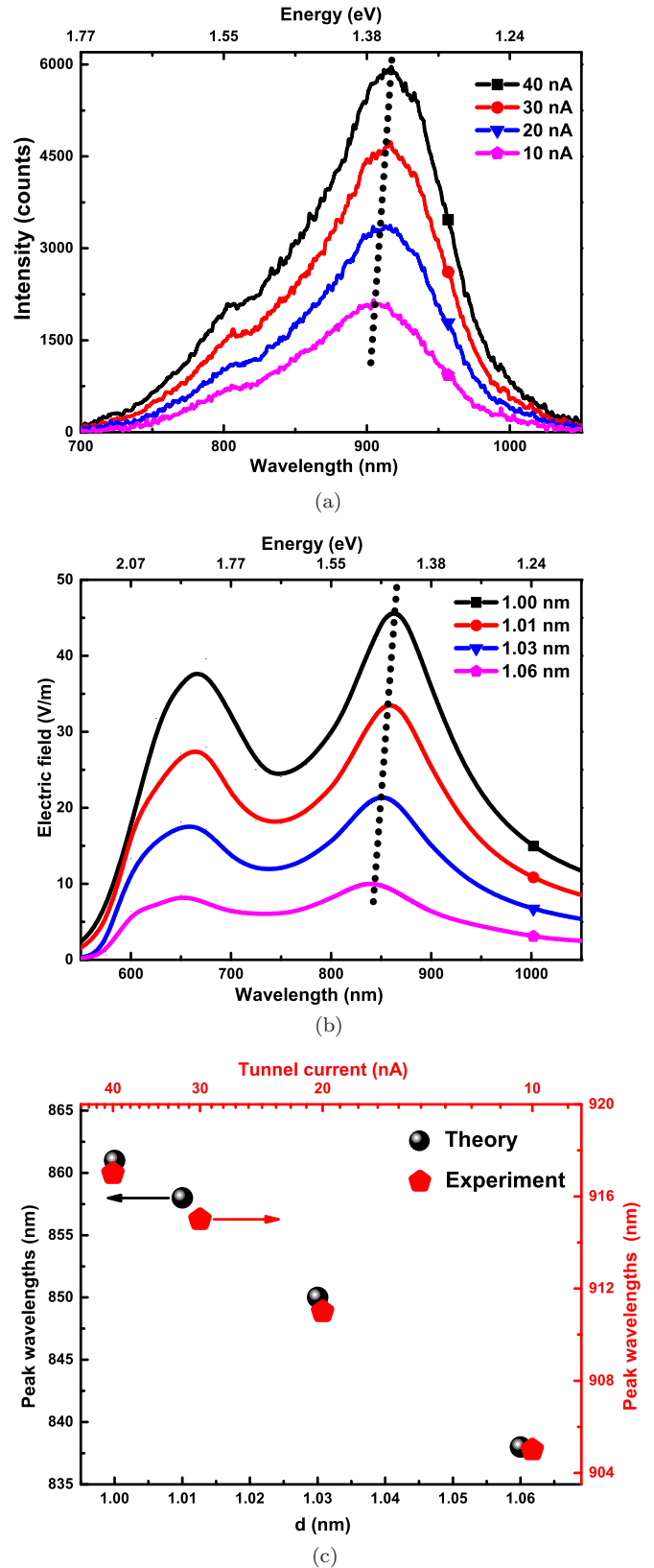
FIG. 4. (a) Emission spectra obtained from Au-Au TSJ for tunnel current varied from 10 to 40 nA (tip radius 10 nm) with fixed bias 1.8 V (main peaks are connected with a dotted line). (b) Calculated electric-field magnitude at TSJ (10-nm tip) for d varied from 1.00 to 1.06 nm. (c) Change in 0th mode position [connected by dotted lines in (a) and (b)] with d from experiment and theoretical calculations.
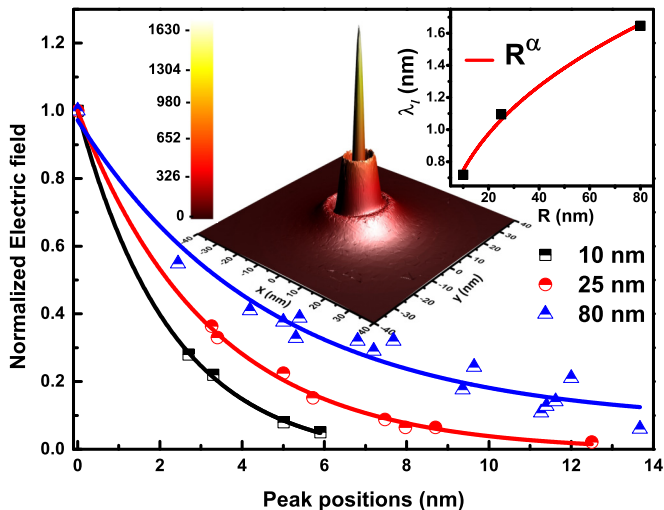
FIG. 5. Normalized peak electric-field values vs lateral peak position, for LSPs (700 nm < λ < 1240 nm), for tips of radii 10, 25, and 80 nm [inset: localization length (λ_l) evaluated as a function of R (see text)]. Red line shows R^α fit to the simulation results. 3D inset: LSP mode excited at TSJ for 80-nm tip at $\lambda = 800$ nm).

for $d/R \ll 1$. The λ_l calculated here varies as $R^{0.4}$ as shown by the fit (red solid line) in the inset. A second inset in Fig. 5 plots the three-dimensional variation of the $|\mathbf{E}_f|^2$ magnitude within the TSJ for the 80-nm tip, with 800-nm excitation. The variation shows that the LSP mode does not decay monotonically, but creates circular-wave-like patterns, which have been reported earlier [35]. It is likely that these symmetric disturbances within the LSP couples on to generate the SPPs that have been detected experimentally from STMLE [19,20].

IV. CONCLUSIONS

In conclusion, we have obtained an expression for the dielectric function of a metal incorporating third-order non-linear corrections, due to a strong dc electric field and theoretically calculated LSP modes of a STM-TSJ to match the experimentally observed STMLE spectra. While it has been known that theoretical calculations assuming the Drude dielectric function do not quantitatively match the experimen-

tal emission spectra, a detailed understanding of the deviation was lacking. Here we discuss the effect of the strong dc electric field permeating the STM junction on the local dielectric properties of the tip and sample. Assuming realistic values for the various parameters involved we demonstrate that the corrections may be strong enough to induce the substantial changes in local dielectric properties such that the ensuing LSP modes match experimental results. Our study provides a recipe for incorporating field dependent local properties that dynamically affect the optical response of the system. The results can be further generalized by incorporating the nonlinear effects of the combined ac and dc fields permeating the junction. Though the model is investigated and discussed in the context of the STMLE the treatment is generically applicable to other examples investigating junction plasmons, where nonlinearity has been known to play a dominant role [62]. Indeed nonlinear plasmonics has recently attracted substantial attention especially in the context of nanophotonics [51]. Crucially, the present model completely ignores the tip-sample charge transfer associated with tunneling. Charge injection into metal nanoparticles, as opposed to charge freezing discussed here, has been shown to have the opposite effect on the plasma frequency, i.e., blueshift with increased charge injection [63]. Thus, future models must incorporate the quantum effects of charge transfer that is central to the STM [46]. In modern photonic applications nonlinear optical properties of the metal nanoparticles and their dependence on the local electric field are highly topical and relevant areas [64,65]. Remarkably, STM is one of the discernible systems in which a metal nanostructure can be controllably positioned over a substrate and vice versa, in an intense electric field, where the plasmonic excitation is achieved by nonoptical means. The STM setup thus provides the ultimate *dark-field* environment to study the weak nonlinear properties of various plasmonic systems.

[1] J. Lambe and S. L. McCarthy, Phys. Rev. Lett. **37**, 923 (1976).

[2] P. Dawson, D. G. Walmsley, H. A. Quinn, and A. J. L. Ferguson, Phys. Rev. B **30**, 3164 (1984).

[3] J. R. Kirtley, T. N. Theis, and J. C. Tsang, Appl. Phys. Lett. **37**, 435 (1980).

[4] J. Kirtley, T. N. Theis, and J. C. Tsang, Phys. Rev. B **24**, 5650 (1981).

[5] S. L. McCarthy and J. Lambe, Appl. Phys. Lett. **30**, 427 (1977).

[6] J. K. Gimzewski, B. Reihl, J. H. Coombs, and R. R. Schlittler, Z. Phys. B: Condens. Matter **72**, 497 (1988).

[7] P. Johansson, R. Monreal, and P. Apell, Phys. Rev. B **42**, 9210 (1990).

[8] R. Berndt, J. K. Gimzewski, and P. Johansson, Phys. Rev. Lett. **67**, 3796 (1991).

[9] P. Dumas, C. Syrykh, I. V. Makarenko, and F. Salvan, Europhys. Lett. **40**, 447 (1997).

[10] A. Downes, M. E. Taylor, and M. E. Welland, Phys. Rev. B **57**, 6706 (1998).

[11] M. Sakurai and M. Aono, Phys. Rev. B **64**, 045402 (2001).

[12] M. Sakurai, C. Thirstrup, and M. Aono, Appl. Phys. A **80**, 1153 (2005).

[13] P. Dawson and M. G. Boyle, J. Opt. A: Pure Appl. Opt. **8**, S219 (2006).

[14] M. G. Boyle, J. Mitra, and P. Dawson, Nanotechnology **20**, 335202 (2009).

[15] N. Nilius, N. Ernst, and H. J. Freund, Phys. Rev. B **65**, 115421 (2002).

[16] G. Schull, M. Becker, and R. Berndt, Phys. Rev. Lett. **101**, 136801 (2008).

[17] J. Steidtner and B. Pettinger, Phys. Rev. Lett. **100**, 236101 (2008).

[18] R. Zhang, Y. Zhang, Z. C. Dong, S. Jiang, C. Zhang, L. G. Chen, L. Zhang, Y. Liao, J. Aizpurua, Y. Luo, J. L. Yang, and J. G. Hou, Nature (London) **498**, 82 (2013).

[19] P. Bharadwaj, A. Bouhelier, and L. Novotny, Phys. Rev. Lett. **106**, 226802 (2011).

[20] T. Wang, E. Boer-Duchemin, Y. Zhang, G. Comtet, and G. Dujardin, Nanotechnology **22**, 175201 (2011).

[21] M. G. Boyle, J. Mitra, and P. Dawson, Appl. Phys. Lett. **94**, 233118 (2009).

[22] T. Lutz, C. Große, C. Dette, A. Kabakchiev, F. Schramm, M. Ruben, R. Gutzler, K. Kuhnke, U. Schlickum, and K. Kern, Nano Lett. **13**, 2846 (2013).

[23] E. L. Moal, S. Marguet, B. Rogez, S. Mukherjee, P. D. Santos, E. Boer-Duchemin, G. Comtet, and G. Dujardin, Nano Lett. **13**, 4198 (2013).

[24] T. Okamoto and I. Yamaguchi, J. Phys. Chem. B **107**, 10321 (2003).

[25] F. Le, N. Z. Lwin, J. M. Steele, M. Kall, N. J. Halas, and P. Nordlander, Nano Lett. **5**, 2009 (2005).

[26] P. Nordlander and F. Le, Appl. Phys. B **84**, 35 (2006).

[27] G. Lévêque and O. J. F. Martin, Opt. Express **14**, 9971 (2006).

[28] F. Le, N. Z. Lwin, N. J. Halas, and P. Nordlander, Phys. Rev. B **76**, 165410 (2007).

[29] C. Ciraci, R. T. Hill, J. J. Mock, Y. Urzhumov, A. I. Fernández-Domínguez, S. A. Maier, J. B. Pendry, A. Chilkoti, and D. R. Smith, Science **337**, 1072 (2012).

[30] S. Mubeen, S. P. Zhang, N. Kim, S. Lee, S. Kramer, H. X. Xu, and M. Moskovits, Nano Lett. **12**, 2088 (2012).

[31] F. Schertz, M. Schmelzeisen, R. Mohammadi, M. Kreiter, H. J. Elmers, and G. Schonhense, Nano Lett. **12**, 1885 (2012).

[32] D. Y. Lei, A. I. Fernández-Domínguez, Y. Sonnefraud, K. Appavoo, R. F. Haglund, J. B. Pendry, and S. A. Maier, ACS Nano **6**, 1380 (2012).

[33] R. W. Rendell and D. J. Scalapino, Phys. Rev. B **24**, 3276 (1981).

[34] L. Tapaszto, G. Dobrik, P. Lambin, and L. P. Biro, Nat. Nanotechnol. **3**, 397 (2008).

[35] J. Mitra, L. Feng, M. G. Boyle, and P. Dawson, J. Phys. D: Appl. Phys. **42**, 215101 (2009).

[36] R. L. Olmon, B. Slovick, T. W. Johnson, D. Shelton, S.-H. Oh, G. D. Boreman, and M. B. Raschke, Phys. Rev. B **86**, 235147 (2012).

[37] E. Prodan, P. Nordlander, and N. J. Halas, Nano. Lett. **3**, 1411 (2003).

[38] M. G. Boyle, L. Feng, and P. Dawson, Ultramicroscopy **108**, 558 (2008).

[39] N. W. Ashcroft and D. N. Mermin, *Solid State Physics* (Harcourt Asia PTE LTD, Singapore, 2001).

[40] P. K. Jain, K. S. Lee, I. H. El-Sayed, and M. A. El-Sayed, J. Phys. Chem. B **110**, 7238 (2006).

[41] V. Myroshnychenko, J. Rodriguez-Fernandez, I. Pastoriza-Santos, A. M. Funston, C. Novo, P. Mulvaney, L. M. Liz-Marzan, and F. J. G. de Abajo, Chem. Soc. Rev. **37**, 1792 (2008).

[42] K.-S. Lee and M. A. El-Sayed, J. Phys. Chem. B **110**, 19220 (2006).

[43] A. Vial, A.-S. Grimault, D. Macías, D. Barchiesi, and M. L. de la Chapelle, Phys. Rev. B **71**, 085416 (2005).

[44] P. B. Johnson and R. W. Christy, Phys. Rev. B **6**, 4370 (1972).

[45] C. F. Bohren and D. R. Huffman, *Absorption and Scattering of Light by Small Particles* (Wiley-VCH Verlag GmbH, Weinheim, Germany, 1998).

[46] K. J. Savage, M. M. Hawkeye, R. Esteban, A. G. Borisov, J. Aizpurua, and J. J. Baumberg, Nature (London) **491**, 574 (2012).

[47] R. Esteban, A. G. Borisov, P. Nordlander, and J. Aizpurua, Nat. Commun. **3**, 825 (2012).

[48] T. Y. Dong, X. K. Ma, and R. Mittra, Appl. Phys. Lett. **101**, 233111 (2012).

[49] R. W. Boyd, *Nonlinear Optics*, 3rd ed. (Elsevier, New Delhi, 2009).

[50] R. W. Boyd, Z. Shi, and I. De Leon, Opt. Commun. **326**, 74 (2014).

[51] M. Kauranen and A. V. Zayats, Nat. Photon. **6**, 737 (2012).

[52] D. Rogovin and D. Scalapino, Ann. Phys. **86**, 1 (1974).

[53] B. K. Juluri, Y. B. Zheng, D. Ahmed, L. Jensen, and T. J. Huang, J. Phys. Chem. C **112**, 7309 (2008).

[54] P. Ginzburg, A. Hayat, N. Berkovitch, and M. Orenstein, Opt. Lett. **35**, 1551 (2010).

[55] N. F. Mott and R. J. Watts-Tobin, Electrochim. Acta **4**, 79 (1961).

[56] J. Aizpurua, S. P. Apell, and R. Berndt, Phys. Rev. B **62**, 2065 (2000).

[57] J. Aizpurua, G. Hoffmann, S. P. Apell, and R. Berndt, Phys. Rev. Lett. **89**, 156803 (2002).

[58] S. C. Lam and R. J. Needs, J. Phys.: Condens. Matter **5**, 2101 (1993).

[59] T. T. Tsong and E. W. Muller, Phys. Rev. **181**, 530 (1969).

[60] F. Hache, D. Ricard, C. Flytzanis, and U. Kreibig, Appl. Phys. A **47**, 347 (1988).

[61] P. Chu and D. L. Mills, Phys. Rev. B **84**, 045430 (2011).

[62] K. Thyagarajan, S. Rivier, A. Lovera, and O. J. F. Martin, Opt. Express **20**, 12860 (2012).

[63] P. Mulvaney, J. Pérez-Juste, M. Giersig, L. Liz-Marzán, and C. Pecharromán, Plasmonics **1**, 61 (2006).

[64] J. Butet, K. Thyagarajan, and O. J. F. Martin, Nano Lett. **13**, 1787 (2013).

[65] J. Butet and O. J. F. Martin, ACS Nano **8**, 4931 (2014).